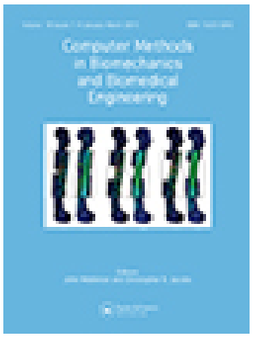

Taylor & Francis
Taylor & Francis Group

Computer Methods in Biomechanics and Biomedical Engineering

ISSN: 1025-5842 (Print) 1476-8259 (Online) Journal homepage: http://www.tandfonline.com/loi/gcmb20

Modelling the glycocalyx–endothelium–erythrocyte interaction in the microcirculation: a computational study

Giuseppe Pontrelli, Ian Halliday, Tim J. Spencer, Carola S. König & Michael W. Collins

To cite this article: Giuseppe Pontrelli, Ian Halliday, Tim J. Spencer, Carola S. König & Michael W. Collins (2015) Modelling the glycocalyx–endothelium–erythrocyte interaction in the microcirculation: a computational study, Computer Methods in Biomechanics and Biomedical Engineering, 18:4, 351-361, DOI: 10.1080/10255842.2013.799146

To link to this article: http://dx.doi.org/10.1080/10255842.2013.799146

Published online: 04 Jun 2013.

Computer Methods in Biomechanics and Biomedical Engineering, 2015
Vol. 18, No. 4, 351–361, http://dx.doi.org/10.1080/10255842.2013.799146

Modelling the glycocalyx–endothelium–erythrocyte interaction in the microcirculation: a computational study

Giuseppe Pontrelli[a]*, Ian Halliday[b1], Tim J. Spencer[b2], Carola S. König[c3] and Michael W. Collins[d4]

[a]*Istituto per le Applicazioni del Calcolo, CNR, Via dei Taurini 19, 00185 Roma, Italy;* [b]*Materials and Engineering Research Institute, Sheffield Hallam University, Sheffield, UK;* [c]*Institute for Bioengineering, Brunel University, London, UK;* [d]*School of Engineering and Design, Brunel University, London, UK*

(*Received 23 July 2012; final version received 22 April 2013*)

A novel, coarse-grained, single-framework 'Eulerian' model for blood flow in the microvascular circulation is presented and used to estimate the variations in flow properties that accrue from all of the following: (i) wall position variation, associated with the endothelial cells' (ECs) shape, (ii) glycocalyx layer (GL) effects and (iii) the particulate nature of blood. We stress that our new model is fully coupled and uses only a single Eulerian computational framework to recover complex effects, dispensing altogether with the need for, e.g. re-meshing and advected sets of Lagrangian points. Physically, blood is modelled as a two-component, incompressible fluid – the plasma and corpuscular elements dispersed in it. The latter are modelled as deformable liquid droplets of increased viscosity. Interfacial membrane effects are present to mimic key blood properties and to avoid droplets' coalescence. The model is encapsulated within a multi-component lattice Boltzmann method that uses a sub-lattice 'wavy wall' closure to represent the ECs. Between this boundary and the flow domain, the model incorporates a coarse-grained representation of the endothelial GL, which is known to cover microvessel walls. The endothelial glycocalyx is modelled as a medium of variable and adaptive porosity, with approaching droplets being subject to a repulsive elastic force. Numerical simulations are presented to show the combined and simultaneous influence on fundamental flow properties of the EC wall undulation, the glycocalyx compression and repulsion and the particulate nature of blood. Several characteristic hemodynamical features of microvessel flow are successfully reproduced, including the deformability of particulates and the Fahraeus–Lindqvist effect. Moreover, the importance of modelling the GL is manifest in the magnitude of and the temporal variations in the flow rate and wall shear stresses.

Keywords: microcirculation; glycocalyx; lattice Boltzmann method; multi-component fluid; endothelium

1. Introduction

The endothelium plays an important role in the vascular system. The shape of the endothelium, or microvessel boundary, is defined by endothelial cells (ECs henceforth), causing the arterial wall to undulate (Figure 1). This effect becomes more pronounced in small-sized vessels, where the corrugation degree, relative to the vessel diameter, increases. Dysfunction of ECs may lead to several pathological states, including, in one example, early development of atherosclerosis (Yao et al. 2007). Hence, it is useful to understand flow properties and forces upon these surfaces. A comprehensive review on the theoretical models in arterial biomechanics, the role of the endothelium in vascular remodelling and the major challenges has been recently developed (Waters et al. 2011).

The presence of an irregular EC surface topography has been addressed by Van Doormal et al. (2009) for cellular mass transfer. Wada and Karino (2002) also studied, theoretically, flows over undulating ECs but with the emphasis on correlating the transport and concentration of low-density lipoproteins at the surface, in relation to wall shear stress variations. Recently, a study of blood flow over a regularly undulating wall, made of uniformly aligned and distributed identical ECs, has been carried out by Pontrelli, König, et al. (2011), who quantify the variation of wall shear stress over the ECs. However, it is well known that the endothelium is coated by long-chained macromolecules, forming a complex protein meshwork that forms a thin porous layer, called the *glycocalyx* (Figure 2) (Weinbaum et al. 2007). The glycocalyx has a 'brush-like' structure and thickness which can vary with the vessel diameter. It has been estimated that the average height of the glycocalyx is ~ 100 nm for arterioles and capillaries (Pahakis et al. 2007). It has several putative roles: it serves as a transport barrier, to prevent ballistic red blood cell (RBC) interactions with the endothelium and as a sensor and transducer of mechanical forces, such as fluid shear stress, to the surface of ECs. Actually, it has been recognised that the glycocalyx responds to the flow environment and, in particular, to the fluid stress, but the mechanism by which these cells sense the shearing forces and transduce mechanical into biochemical signals is still not fully understood (Pahakis et al. 2007; Weinbaum et al. 2007). It has been reported that the glycocalyx itself is remodelled by the shearing flow and by the compression exerted by the

*Corresponding author. Email: giuseppe.pontrelli@gmail.com

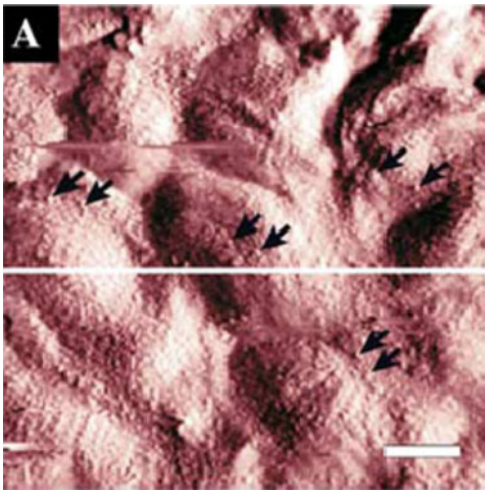

Figure 1. An experimental (optical microscope) image of the rough, or 'wavy', surface of an arterial wall comprised of tessellating ECs (courtesy of Reichlin et al. 2005). The no-slip boundary condition used in this work is a 2D representation of this surface. The solid arrows point to ECs; the scale bar corresponds to 5 μm.

deformed erythrocytes or RBCs in capillaries (Secomb et al. 2002).

Over the years, flow-induced mechano-transduction in ECs has been studied in order to find correlations between disturbed flow patterns and atherosclerosis. Such studies often use 'simple' traditional computational fluid dynamics techniques, which neglect the influence of the glycoclyx layer and the particulate nature of the blood flow, above this layer. Recently, sophisticated immersed boundary methods that combine a lattice Boltzmann (LB) approach with the deformability of RBCs in a shearing flow have been presented by Zhang et al. (2008) and by Krüger et al. (2011) in order accurately to calculate particulate flow effects. Farhat et al. (2011) propose a multi-component model with a non-uniform local interface tension, which accounts for the RBC deformability. Other recent works make use of LB techniques for large-scale simulations of complex hemodynamic flows (Bernaschi et al. 2009), with the inclusion of RBCs as suspended rigid bodies (Janoschek et al. 2010; Melchionna 2011). On the other hand, some modelling work has been carried out by Arslan (2007) and Vincent et al. (2008), who used a porous medium approach to model the glycocalyx layer (GL henceforth). However, none of these works combines the influence of the effect of the endothelial roughness, or 'wavy' nature, of the wall, together with the particulate nature of the flow, and the porous GL. Such a detailed model, combining the above techniques, would provide an accurate but computationally demanding method. In order to provide what is still an accurate picture of flows within the microcirculation, these effects are, here, approximated further and efficiently combined within a single Eulerian framework, with the purpose of defining to produce a relatively simple, accessible and novel coarse-grained model, capable of investigating, and providing an estimate of, the variations in microvascular circulation transport properties.

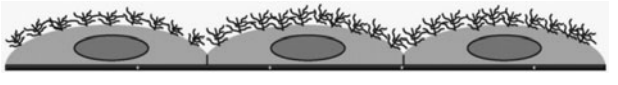

Figure 2. The 'brushlike' structure of the glycocalyx over the wavy wall constituted by a sequence of equally aligned ECs (courtesy of Yao et al. 2007).

In the following sections, we present the new coarse-grained model that attempts to include, within a single, unifying framework, all the pertinent microscale physical effects, but most novel, the GL attached to the EC surface. The inherent versatility of the LB method will be seen as central to our work. We then examine the extent to which wall shear stress may vary, due to the GL, in addition to the previously examined EC shape and particulate transport. To model blood flow in small-sized arteries, the mesoscopic multiple-immiscible fluid LB method is used (Pontrelli, Halliday, et al. 2011; Pontrelli, König, et al. 2011). To facilitate the analysis, the present model includes a representation of the EC's shape through a periodic 'wavy wall'; this geometry is combined with a multi-component flow model of viscous fluid droplets, with interfacial surface tension and, finally, with a representation of the GL that considers both the effect upon the particles and the fluid transport properties.

2. Blood flow in small-sized arteries and capillaries

In many studies of haemodynamics, blood is assumed to be an incompressible, Newtonian fluid and the arterial wall to be flat. The first assumption ignores the non-Newtonian effects and the particulate nature of the blood, and the latter neglects the microscale undulation of the wall due to the shape of the influence of constituent ECs: this does not imply a significant variation in the flow field, but it is relevant in computing wall shear stress (WSS), which is constant in a flat-walled artery. In fact, the internal surface of the vessel wall is covered by a sequence of ECs, forming a continuous, wavy layer. A single EC has been estimated to be about 15 μm long by 0.5 μm high (Reichlin et al. 2005) (Figure 1). At such a scale, the wall may be considered as a smoothly corrugated idealised no-slip surface, constituted by a regular array of equal, repeated ECs (Figures 2 and 3). The pressure-driven axi-symmetric flow of a continuum fluid over such a surface has been recently modelled by Pontrelli, König, et al. (2011). It was shown that, despite no significant change in velocity profiles, significant WSS variations can occur

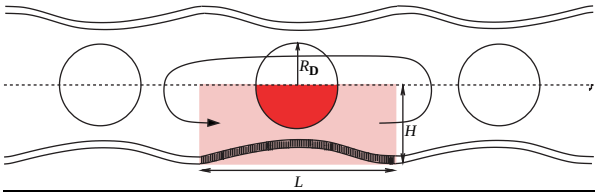

Figure 3. Schematic diagram of the model system. Exploiting axi-symmetry, flow in a half-channel, H, is considered. Periodic boundaries are used over the length, L, of one EC, so only a portion of the vessel is considered explicitly (grey region). The hatched layer near the wall indicates the glycocalyx, and the arrow-headed line is used to emphasise the periodic boundary conditions for particles at the inlet–outlet regions implemented in our simulations. Gradients vanish on the central symmetry axis (figure not to scale).

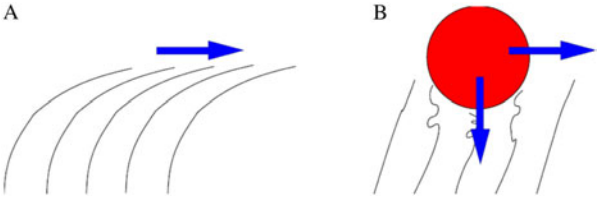

Figure 4. A representation of the assumed mechanical properties of the glycocalyx protein chains, subject to a streaming flow only (A) and direct interaction with a flow-advected particulate (B). Note that the principal deformation is assumed to be confined to the tip of the filaments, adjacent to the lumen (figure not to scale).

between the EC boundary peaks and throats, especially in small-sized arteries. Here, we extend this work in two main ways. First, the particulate nature of the fluid is included, by considering the fluid plasma to be made up of separated erythrocytes, each approximated, coarsely but very efficiently, as deformable, neutrally buoyant immiscible liquid drops, with a uniform interfacial tension relative to the embedding 'plasma' fluid. Second, the endothelial glycocalyx and its coupling to the erythrocyte, or drop, is also included (see Section 3). In the current formulation presented here, a single file of erythrocytes (due to the periodic boundaries) flow in a narrow arteriole, each with their centre of gravity located on the symmetry axis and their degree of deformation is seen to be similar to those geometrically confined within capillaries (Secomb et al. 2002). We consider a two-dimensional (2D) axi-symmetric channel, having the same corrugation repeated along its length, and a semi-height H. For the sake of simplicity, a single EC is considered and periodic boundary conditions are imposed, in order to model an infinitely long channel (Figure 3). In a Cartesian coordinate system with x-horizontal, y-vertical, the domain is defined as $[0, L] \times [0, H]$. A single circular droplet of initial radius R_D is placed in the plasma, centred on the system symmetry line (Figure 3).

3. A coarse-grained model of glycocalyx effects

As mentioned earlier, the endothelial surface is not only wavy in its geometry, but, at a smaller scale, it is known to be covered by fibrous filaments and long protein chains, forming a thin protein meshwork layer, called the *endothelial surface layer* or *glycocalyx*. From a continuum fluid dynamics point of view, the GL may be modelled as a porous layer (Arslan 2007; Vincent et al. 2008) nominally of constant thickness (but see below), which follows the wall undulation, through which the flow of the continuous phase (plasma) is possible. This alters the boundary conditions of the problem, specifically the usual no-slip condition at the vessel wall has to be replaced, to model plasma penetration through the GL and endothelial clefts. We choose to embed the GL in our model within the framework of LB method, which readily accommodates multiscale, multi-physics modelling. Essentially, the idea here is to solve a multiple-domain problem, in which an 'inner' or 'bulk' multi-component flow, in the microvessel lumen, is described by the Navier–Stokes equations and interfacial boundary conditions consistent with a blood cell representation as a liquid drop and, in the near-wall region, single-component flow (of the plasma component only) is described by a porous-medium, Brinkman flow formulation discussed below. Crucially, one particular multi-component LB method can be straightforwardly adjusted to represent both bulk and near-wall flow. At the microscale, the glycocalyx is not modelled in its detailed structural form, but its effect on the flow is still properly addressed (using methods that, for example, are amenable to subsequent calibration, using more detailed, simulations and experiments, located on shorter length and time scales). A 'two-way coupled' model can be possible, in which the drop interface is forced by ballistic contact with a compression of the GL, and this effect is then communicated to the flow (Figure 4). In the present article, however, the latter effect is not included and will be considered in a future publication that deals in more detail with the near wall region alone. The nonlinear mechanical response of the GL to RBC's ballistic impact is a complex and challenging issue, and the appropriate approximations that are made here must eventually be verified by experimental microscale studies.

4. Formulation of the problem

We employ the meso-scale LB method to solve all the governing hydrodynamic equations in our model that, recall, also involves multi-component fluid flow, off-lattice or sub-grid, boundary surfaces and a porous-layer representative of the GL.

The governing hydrodynamic equations for flow in a porous media, with constant or variable porosity, $\varepsilon(\underline{x})$, as presented in Guo and Zhao (2002), are:

$$\nabla\cdot\underline{u} = 0, \tag{1}$$

$$\frac{\partial \underline{u}}{\partial t} + (\underline{u}\cdot\nabla)\left(\frac{\underline{u}}{\varepsilon}\right) = -\frac{1}{\rho}\nabla(\varepsilon P) + \nu\nabla^2\underline{u} + \underline{F}(\varepsilon) \tag{2}$$

Here ρ, $\underline{u}$ and P are the fluid density, velocity and pressure respectively, ν is the effective fluid viscosity and the function $\underline{F}(\varepsilon)$ is the total body force with several contributions:

$$\underline{F}(\varepsilon) = -\frac{\varepsilon\nu}{K}\underline{u} - \frac{\varepsilon F_\varepsilon}{\sqrt{K}}\underline{u}|\underline{u}| + \varepsilon\underline{G}. \tag{3}$$

In Equation (3), $K = \varepsilon^3 d^2/150(1-\varepsilon)^2$ is the permeability, d is the property of the porous structure, $F_\varepsilon = 1.75/\sqrt{150\varepsilon^3}$ is the geometrical function and $\underline{G}$ is the additional body force used to incorporate further details of the GL and the interfacial immersed boundary force density which acts between the drop and embedding fluid (Halliday et al. 2007), when the embedding fluid occupies the GL domain. This force is further discussed below, and the other terms represent the presence of porous material.

In a two-way coupled model, any ballistic contact between the immersed boundary and GL will produce compression of the latter. By computing the loss of volume (or, in 2D, of area) in the GL domain which results from such a contact, it is, in principle, straightforward to compute a local increase of the GL material density and, hence, to determine a local perturbation in the porosity, $\varepsilon(\underline{x})$, which might be applied in Equations (1)–(3). In this way, a two-way coupling could be introduced, though the observation of its effects is likely to require simulations on smaller scales than those we pursue here. Hence, we proceed, in this article, with a static porosity, $\varepsilon(\underline{x})$.

To solve the governing Equations (1)–(3) and to include particulate components, we combine the LB methods of Guo and Zhao (2002), with the model of Halliday et al. (2007). The latter allows for the introduction of two immiscible fluid components and the formation of diffused interfaces that embed correct kinematic and interfacial surface tension laws to efficiently approximate the particulate effects. However, it is noted that this first-order approximation does not include a cell membrane bending rigidity or surface area conservation constraint that is associated with erythrocytes. Including such effects would obviate the simplicity and efficiency of the proposed model whilst only making relatively minor quantitative differences to the subsequent WSS calculations. Following the notations of those papers, the resultant LB algorithm for the particle distribution functions, $f_i(\underline{x},t)$, at position $\underline{x}$, time t and lattice link direction i, is written as an evolution process comprised of a collision and a propagation:

$$\begin{aligned} f_i^+ &= f_i(\underline{x}, t+\Delta t) \\ &= f_i(\underline{x},t) - \frac{1}{\tau}(f_i(\underline{x},t) - f_i^{\mathrm{eq}}(\underline{x},t)) + \Delta t F_i, \end{aligned}$$

that is further discussed below. In the last equation, the equilibrium distribution function, f_i^{eq}, and lattice source term, F_i, are defined, respectively, as

$$f_i^{\mathrm{eq}}(\underline{x},t) = t_i\rho\left(1 + \frac{\underline{e}_i\cdot\underline{u}}{c_\mathrm{s}^2} + \frac{\underline{u}\,\underline{u}\left(\underline{e}_i\underline{e}_i - c_\mathrm{s}^2\underline{\underline{I}}\right)}{2\varepsilon c_\mathrm{s}^4}\right),$$

$$F_i(\underline{x},t) = t_i\rho\left(1-\frac{1}{2\tau}\right)\left[\frac{\underline{e}_i\cdot\underline{F}}{c_\mathrm{s}^2} + \frac{\underline{u}\cdot\underline{F}\left(\underline{e}_i\underline{e}_i - c_\mathrm{s}^2\underline{\underline{I}}\right)}{\varepsilon c_\mathrm{s}^4}\right].$$

In these equations, $\underline{\underline{I}}$ is the identity matrix, $\underline{e}_i$ and t_i are, respectively, the lattice basis vectors and their associated weights, c_s is the speed of sound of the LB model lattice used, and τ is the relaxation parameter, related to the simulated fluid viscosity (Succi 2001). The $1-1/2\tau$ prefactor and denominator ε in these equations occur as a direct result of using the LB method and ensure the correct recovery of the target macroscopic equations. Full details are given in Guo et al. (2002) and Guo and Zhao (2002), respectively. The density, ρ, final velocity, $\underline{u}$, fluid pressure, P and kinematic viscosity, ν, in our particular LB model, are expressed in dimensionless lattice units, respectively, as:

$$\rho = \sum_i f_i(\underline{x},t),$$

$$\underline{u} = \frac{\underline{\mathrm{v}}}{p_0 + \sqrt{p_0^2 + p_1|\underline{\mathrm{v}}|}},$$

$$P = \rho c_\mathrm{s}^2,$$

$$\nu = \frac{\Delta t c_\mathrm{s}^2}{2}(2\tau - 1),$$

in which the following auxiliary quantities are implicit (Guo and Zhao 2002):

$$\rho\underline{\mathrm{v}} = \sum_i \underline{e}_i f_i(\underline{x},t) + \frac{\Delta t}{2}\varepsilon\rho\underline{G}, \quad p_0 = \frac{1}{2}\left(1 + \frac{\varepsilon}{2}\frac{\nu}{K}\right),$$

$$p_1 = \left(\frac{\varepsilon}{2}\frac{F_\varepsilon}{\sqrt{K}}\right).$$

To complete our account of the algorithm, we must mention that, for multiple fluid LB, the propagation step is augmented by a fluid segregation process (Halliday et al. 2007), which ensures the correct kinematics and dynamics as well as the integrity of the emergent interface between the completely immiscible fluid components used to

represent our particulates, as discussed above. The appropriately extended propagation step is expressed as:

$$R_i(\underline{x}+\underline{e}_i\Delta t, t+\Delta t) = \frac{R}{\rho}f_i^+ + t_i\beta\frac{RB}{\rho}\hat{\underline{n}}\cdot\underline{e}_i,$$
$$B_i(\underline{x}+\underline{e}_i\Delta t, t+\Delta t) = \frac{B}{\rho}f_i^+ - t_i\beta\frac{RB}{\rho}\hat{\underline{n}}\cdot\underline{e}_i, \quad (4)$$

where the density of each fluid component is given by $R=\sum_i R_i(\underline{x},t)$ and $B=\sum_i B_i(\underline{x},t)$ and the combined particle distribution function is $f_i(\underline{x},t)=R_i(\underline{x},t)+B_i(\underline{x},t)$, β is an interfacial segregation parameter, and $\hat{\underline{n}}$ is an interfacial unit normal vector. We also note that, if only one fluid component exists, Equation (4) reduces to the standard LB propagation step.

Returning to the definition of the extra body force term, $\underline{G}$ in Equation (3), this incorporates both particulate and glycocalyx forces and is defined as

$$\underline{G} = \frac{\sigma}{2\rho}\pi\nabla\rho_N + \underline{E}.$$

The left-hand side term imposes interfacial tension, σ, on deformable particles (i.e. droplets). Here, $\pi=\nabla\cdot\hat{\underline{n}}$ is the local curvature and $\rho_N=(R-B)/(R+B)$ is a phase field indicator. The right-hand term, $\underline{E}$, is a glycocalyx force that acts upon the particles as defined in Section 5.

It is important to point out that the necessary off-lattice, no-slip endothelial surface boundary condition uses continuous bounce back lattice closure conditions (Bouzidi et al. 2001), and the pressure-driven flow is enforced at the inlet–outlet by use of extended periodic boundary conditions (Kim and Pitsch 2007) that allow a pressure step to be defined. A symmetric condition is imposed at the centerline.

It is noted that, in contrast to other methods, the approach and approximations adopted here dispense with the need to track explicitly the RBC membranes and result a computationally inexpensive and simple algorithm within a single framework.

5. A model of erythrocytes–glycocalyx interaction

In our model of the GL as a porous layer, one consequence of ballistic contact with an erythrocyte is that the GL is squashed, transporting the same protein filament mass into a smaller volume, decreasing its porosity. As discussed in Section 4, a geometrical model of what is an easy-to-model volume exclusion effect could be used to construct a local, contact-induced GL porosity variation. However, we adopt a 'light encounter' model and assume that such an effect is small on the spatial and temporal scales of interest here.

Even in the simplest situation, the GL-lumen boundary should not be regarded as sharp, and there is an 'uncertainty' region between bulk, lumen and glycocalyx material. For this reason, a variable porosity, $\varepsilon(x, y)$, is defined. This quantity tends to a value of 1 in the lumen region and gradually reduces, on entering the GL region, where it approaches a minimum value, ε_G. This porosity transition is modelled through the increasing smooth function:

$$\varepsilon(x,y) = \varepsilon_G + \frac{1-\varepsilon_G}{2}[1+\tanh[\xi(s-l)]], \quad (5)$$

where l is the mean GL thickness and the parameter $1/\xi$ determines the distribution of (i.e. the effective standard deviation of) protein chain lengths, while $s(x, y)$ denotes the distance measured in the direction perpendicular to the endothelial boundary. Note that $\varepsilon_G \le \varepsilon(x,y) \le 1$ (Figure 5) and that for $\varepsilon \to 1$, we have $\underline{F} \to \underline{G}$ and Equations (1)–(3) reduce the multi-component LB Navier–Stokes equations for incompressible fluids.

Consider a drop interface impinging on the GL from the lumen. As the model GL is squashed, an additional, fictitious, repulsive body force density acts on any part of the interface which enters the GL region. This force distribution is so designed that its accumulation produces an effective Hookean force, acting at the centre of the local volume. Put another way, the drop-erythrocyte surface is locally subjected to a surface force distribution, effective in the GL only, which is directed everywhere in the drop-surface normal direction. This force device effectively models the glycocalyx as a continuum of elastic springs,

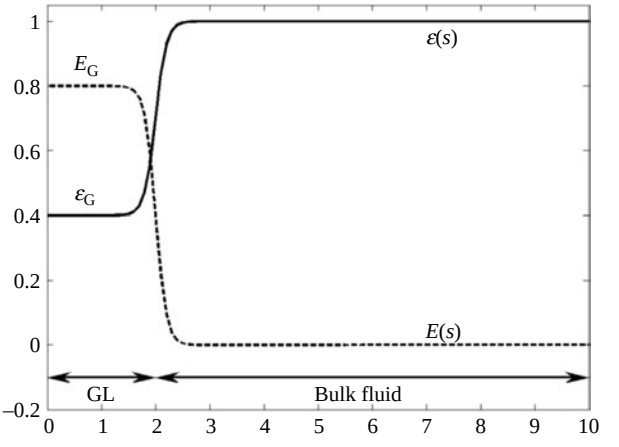

Figure 5. The porosity (continuous line) as a function of s, dimensionless perpendicular lattice distance from the endothelial surface. The former increases from a minimum value ε_G (in the GL), to the bulk fluid ($\varepsilon = 1$) (see Equation (5)). Similarly, the elasticity modulus E (dashed line) varies from a maximum value E_G in the GL to 0 (no elastic force) out of it (see Equation (6)). Note the smooth transition area (due to the uncertain GL thickness) that is controlled by the parameter ξ.

with a modulus E, the value of which gradually decays from a maximum value, E_G (in the GL) to 0 in the lumen, or bulk:

$$E(x, y) = \frac{E_G}{2}[1 - \tanh[\xi(s - l)]], \tag{6}$$

where all notations correspond to Equation (5) (see Figure 5). It is important to note that the above force acts solely on the supernatant fluid (drop) and not upon the plasma. Hence, the relative density of the material which comprises the drop may be modelled by appropriate choice of the spring constant E_G in Equation (6).

6. Numerical results and discussion

As discussed earlier, it is clear that the model and, therefore, its data depend on several parameters. Some relate to the key physical, geometrical or physiological details in the model (note, all are, in principle, obtainable from experiments).

For purposes of systematic analysis, we model a capillary flow after Secomb et al. (2002) by considering a channel with the following regularly corrugated surface that corresponds to a uniform sequence of ECs of length λ and height A:

$$H(x) = H_m + A\cos(\lambda x), \qquad H_m = 3.2\,\mu\text{m}, \quad A = 0.5\,\mu\text{m}, \quad \lambda = 10\,\mu\text{m}. \tag{7}$$

Hence, the boundary is a smooth profile constituted by a series of peaks and valleys: the channel has a varying diameter $2H$ in the range 5.4–7.4 μm and a corrugation degree of $A/H_m = 0.15$ (Secomb et al. 2002). The simulated domain has a length $L = \lambda$ and the GL thickness is $l = 0.7$ μm. A single droplet of radius $R_D = 3.278$ μm is placed in the middle of the channel and subjected to a horizontal pressure gradient, $\Phi = 0.05\,10^{-4}\,\text{dyn}/\mu\text{m}^3$, acting in a tube with diameter $2H = 5$ μm and a Newtonian fluid flow, a mean flow velocity of $U = 128\,\mu\text{m/s}$ (see Section 2 and Figure 3) is set. The kinematic viscosity of the plasma is assumed to be $\nu = 0.01\,\text{cm}^2/\text{s}$.

To obtain the same flow regime, the classical single relaxation time D2Q9 LB lattice scheme designated Lattice Bhatnagar-Gross-Krook (LBGK) (Succi 2001) in a multi-component form (Halliday et al. 2007) is chosen, with the following dimensionless lattice parameters:

$$\tau = 1.25, \quad \rho = 1.8, \quad \beta = 0.67, \quad L = 300,$$

$$H = 111, \quad U = 7.2 \times 10^{-3}, \quad R_D = 98.3,$$

while the porous medium coefficients used are those exactly given as in Guo and Zhao (2002), with a Darcy number $\text{Da} \cong 10^{-4}$. We note that, since in the present application the fluid velocity is quite small, the contribution from the nonlinear drag term in Equation (2) will be negligible, thus reducing Equation (2) to the Brinkman-extended Darcy equations. Certain other parameters are artefacts of the numerical method of our 'coarse-grained' mesoscale glycocalyx model. They are thus designated as 'microscopic' and quantified as follows:

$$\xi = 3, \quad l = 21, \quad E_G = 0.01, \quad \varepsilon_G = 0.6.$$

Of course, all of the latter might be estimated by fitting experimental/microscale simulation data. For example, the standard deviation ξ could, with appropriate effort, be measured from a representative sample of protein chain lengths, l, obtained from microscope images; the effective elasticity constant from fits to explicit microscale simulation data. All the above parameters are chosen to be of a correct order to approximate a physical glycocalyx. These parameters are seen to produce an observable effect on the flow in the region of the drop and must be further quantified (or, at least, bounded within an appropriate range) to produce quantitative data. It is important to note that the stability of simulations may be affected by the combination of the parameters as chosen, which limits the

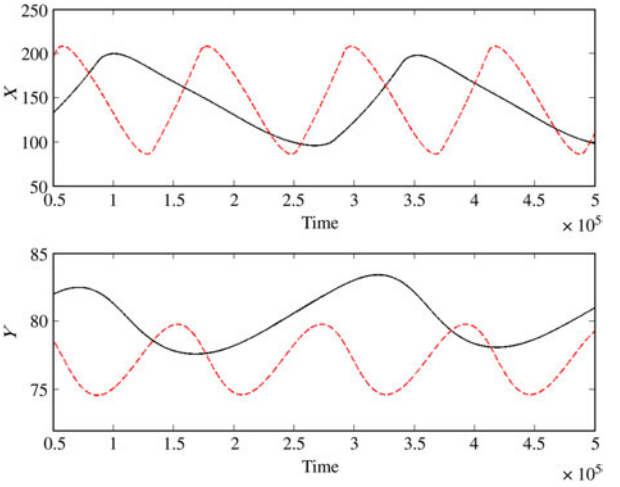

Figure 6. The droplet's centre of mass coordinates versus time [with GL (continuous black line) and without GL (dashed red line)] (LB units). Note the centre of mass coordinates is calculated only over the half space of the simulation domain. In a flow driven by a constant pressure gradient, the oscillation depends on the wall profile undulation and the alternation of sign is a model artefact due to the periodic boundary conditions. The steepest positive slope of the X curve corresponds to the drop's transit over the peak, and the steepest negative slope corresponds to the drop's transit in the valley. In the case with the GL, the reduced slope of $X(t)$ (in a transit segment) estimates the droplet's decreased mean speed, and the larger value Y indicates a drop's lifting over the GL.

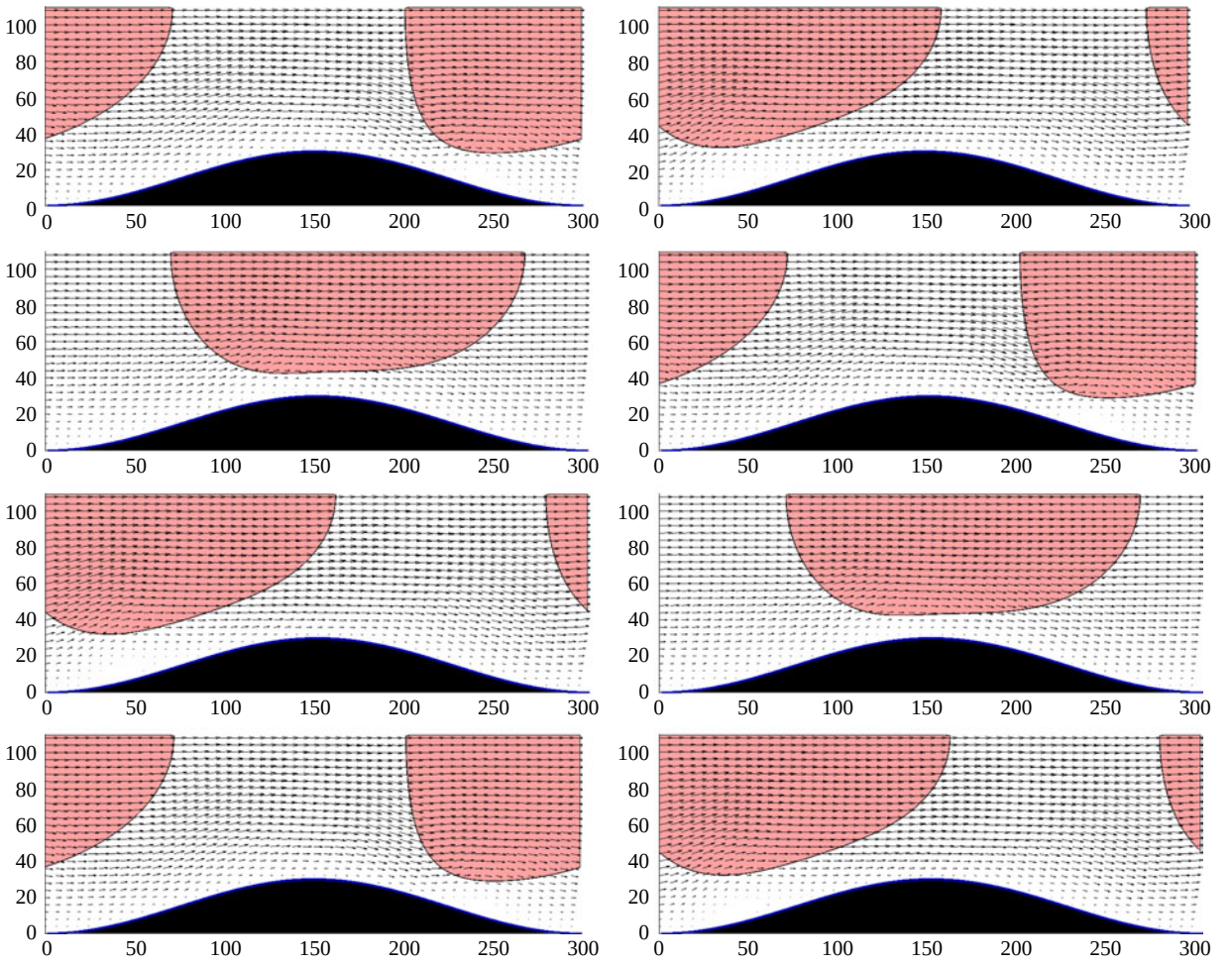

Figure 7. The flow field for the 'aggregate' fluid (drop and supernatant fluids combined) in the region of the endothelium (case without GL) at the eight instants $[20{:}4{:}48] \times 10^4$.

available parameter space for simulation. However, tests indicate an encouragingly robust simulation system, with a large and accessible parameter space, probably as a consequence of the small Re.

We shall consider the flow-induced effects due to the presence (or absence) of the GL with the above chosen parameters of elastic coefficient E_G (see Equation (6)), and the porosity function ε_G (see Equation (5)). As one may expect, the average velocity of the drop is smaller in the presence of the glycocalyx, which constitutes a hindrance on the lumen flow. Figure 6 clearly illustrates this fact. Moreover, the mean deformation of the drop is more pronounced in the presence of the glycocalyx force (Figures 7 and 8). This is apparent in the difference between the average y coordinates recorded for the drops with and without the glycocalyx force present. Hence, when the drop is in the GL influence region, it is subjected to the elastic force, which squeezes and lifts it, away from the boundary, whilst making its shape more elongated (Figures 7 and 8).

Concerning forces acting on the endothelium, there are various classes of mechanical stresses associated with the undulated wall and suspended RBCs. The vessel wall is sheared by the RBC and compressed by the pressure exerted by plasma and cells. The shear stress fluctuates in magnitude and direction from point to point and changes in time. In considering the action of the glycocalyx as a sensor of mechanical forces, it is interesting to compute the shear stress at the GL/lumen interface (GSS). Figure 9 shows the differences for WSS in the cases without and with glycocalyx: it evidences, in the latter case, a reduction of the shearing stress, either at the wall (WSS, due to the plasma only) and at the GL top (GSS, due to the particulate fluid). It is possible that the GL would be more likely to protect the ECs from WSS fluctuations associated with particulate cell transits.

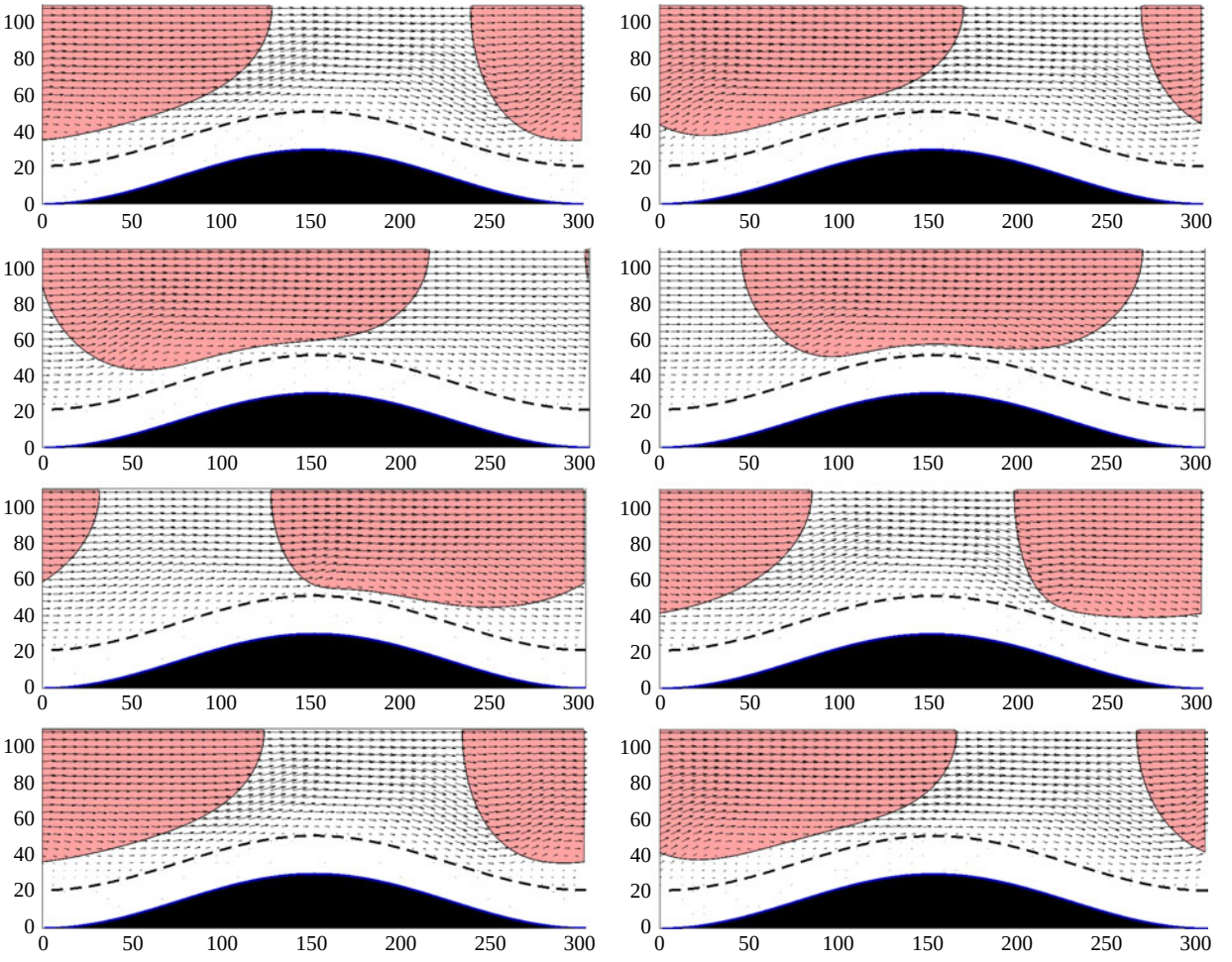

Figure 8. The flow field as before in the presence of GL (the extent of the GL is indicated by the dashed line) at the eight instants $[20{:}4{:}48] \times 10^4$ (cf. with Figure 7). The single deformable drop travelling over the endothelium has been acted on and deformed by encountering the GL body force field. The flow appears to be deflected up which would tend to protect the EC surface from increased WSS.

Consider the volumetric flow rate Q in the 2D wavy channel (in the case of particulate fluid and drop only fluid), which are computed, respectively, as:

$$\begin{aligned} Q_{\mathrm{b}} &= \frac{\int_0^L \mathrm{d}x \int_{H_1}^{H_2} v(x,y)\,\mathrm{d}y}{L}, \\ Q_{\mathrm{c}} &= \frac{\int_0^L \mathrm{d}x \int_{H_1}^{H_2} v(x,y) H^*(x,y)\,\mathrm{d}y}{L}, \end{aligned} \tag{8}$$

where $H_1(x)$ and $H_2(x)$ are the lower and upper wall boundaries, respectively, and

$$H^*(x,y) = \begin{cases} 1, & \text{if } (x,y) \text{ is in a RBC}, \\ 0, & \text{otherwise}. \end{cases}$$

Similarly, the averaged velocities of blood and of RBC are, respectively, as follows:

$$\begin{aligned} \tilde{v}_{\mathrm{b}} &= \frac{\int_0^L \mathrm{d}x \int_{H_1}^{H_2} v(x,y)\,\mathrm{d}y}{\int_0^L \mathrm{d}x \int_{H_1}^{H_2} \mathrm{d}y}, \\ \tilde{v}_{\mathrm{c}} &= \frac{\int_0^L \mathrm{d}x \int_{H_1}^{H_2} v(x,y) H^*(x,y)\,\mathrm{d}y}{\int_0^L \mathrm{d}x \int_{H_1}^{H_2} \mathrm{d}y}. \end{aligned} \tag{9}$$

These quantities depend on the relative position of the deforming drop with respect to the undulated endothelium, and, hence, have an oscillatory behaviour. Taking, for definiteness, the image of a drop travelling across peaks and valleys, the flow rate Q is a maximum when the drop passes over a peak, whereas it reaches a minimum value

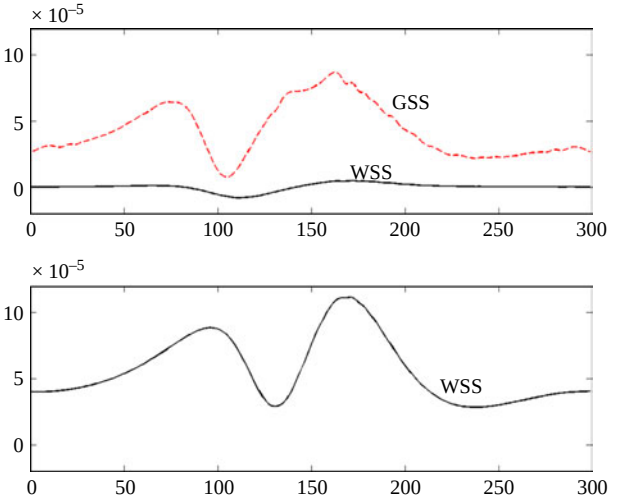

Figure 9. The GSS and WSS over the periodic surface of an EC in the case with GL (top) and without GL (bottom) (LB units). There is a sensible reduction of the value at the endothelium in the first case, due to the protective action of the GL. The two figures are relative at instants such that the drop is in the same position during its transit.

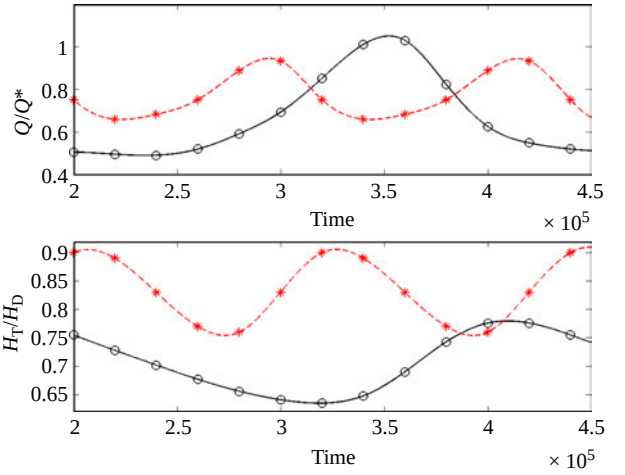

Figure 10. The blood flow rate (Q) (top), the hematocrit ratio (H_T/H_D) (bottom) with GL (continuous black line) and without GL (dashed red line). These quantities depend on the relative position of the drop with respect to the undulated wall and hence show an oscillatory behaviour.

when the drop is above the throat (Figure 10(a)): this aspect is often not explicitly resolved at all, or it appears to be underestimated in other works, particularly those which uses the continuum approximation.

The apparent viscosity of the particulate flow can be obtained by assuming a Poiseuille relation between the applied constant pressure gradient $\Phi = (\Delta p/L)$, and the flow rate, Q. We have the following general relation:

$$\Phi = kQ\nu, \tag{10}$$

where k is a constant depending on the geometry only, while Q and ν depend on the flow configuration. In the case of the same geometry with plasma only (starred case), driven by the same pressure gradient Φ:

$$\Phi = kQ^*\nu^*. \tag{11}$$

From Equations (10) and (11), we have the familiar relationship (Pries and Secomb 2008):

$$\frac{\nu}{\nu^*} = \frac{Q^*}{Q}. \tag{12}$$

In fact, from simulation, it appears that Q^* is constant in space and time in both cases, with a glycocalyx (subscript G) and without it (subscript NOG) having the values:

$$Q^*_{\mathrm{G}} = 0.207, \quad Q^*_{\mathrm{NOG}} = 0.439,$$

In the case of a particulate fluid, Q changes with time (Figure 10(a)) and its average over a 'period' is measured as:

$$\tilde{Q}_{\mathrm{G}} = 0.13, \quad \tilde{Q}_{\mathrm{NOG}} = 0.33.$$

The relative ratio is:

$$\frac{Q^*_{\mathrm{G}}}{\tilde{Q}_{\mathrm{G}}} = 1.59, \quad \frac{Q^*_{\mathrm{NOG}}}{\tilde{Q}_{\mathrm{NOG}}} = 1.33.$$

It turns out that the presence of cells increases the apparent viscosity and this effect is further enhanced by the GL. Because resistance in a viscous flow is defined as $\Delta p/Q$, it follows that the ratio Q^*/Q in the Equation (12) measures also the increase in resistance, for the case of particulate flow, over that of plasma only (Figure 10).

Another issue worth consideration in our explicitly resolved suspension is the *tube hematocrit*, H_{T}, representing the fraction of RBC's volume (V_{c}) over the total blood volume (V_{b}) (Pries and Secomb 2008). In this case:

$$H_{\mathrm{T}} = \frac{V_{\mathrm{c}}}{V_{\mathrm{b}}} = 0.39.$$

The *discharge hematocrit* H_{D} is defined as

$$H_{\mathrm{D}} = \frac{Q_{\mathrm{c}}}{Q_{\mathrm{b}}} = \frac{H_{\mathrm{T}} v_{\mathrm{c}} H}{v_{\mathrm{b}} H},$$

that is

$$\frac{H_{\mathrm{T}}}{H_{\mathrm{D}}} = \frac{v_{\mathrm{b}}}{v_{\mathrm{c}}}.$$

This ratio, which oscillates as long as the RBC travels over the endothelium, is always <1 (Figure 10(b)). The consequence of this fact is a reduced RBC concentration in the slow-moving regions adjacent to the wall and a lateral

migration towards the centre (Fahraeus–Lindqvist effect) (Pries and Secomb 2008). These results are in agreement with those in Secomb et al. (2002) and Farhat et al. (2011), and they demonstrate that our model, though restricted to a 2D case, is able to capture important effects in microvascular flows. Contrary to large-scale simulations, where blood cells can be adequately modelled as rigid particles (Melchionna 2011), the present analysis proves that the wall corrugation, together with the cell deformability, plays an important role in micro-hemodynamics.

7. Conclusions

The endothelial glycocalyx is often seen as a sensor and transducer of mechanical forces. Its role is posited as crucial in enabling the ECs to respond to fluid shear forces. In this work, a single-framework, highly flexible coarse-grained model, able to investigate flow properties and shear stress variations over the interacting endothelial surface, GL and the erythrocyte surface, in the microvascular circulation, has been presented and demonstrated. Our fully coupled model includes, specifically, the wall's EC shape, a porous medium representation of the glycocalyx that follows the EC shape and a representation of the particulate effects of blood. The model has been implemented within the efficient multi-component LB framework (alone) and has been used to highlight the differences that arise if flow parameters and forces, such as the flow rate, shear stress and hematocrit, are considered in the presence and absence of a modelled GL. It is seen that a modelled GL alters both the magnitude and temporal variations in the flow parameters and, as such, should always be considered when interpreting flow data from the microcirculation for clinical use.

Further work on the model can be carried out by performing simulations at a larger scale, in three dimensions, by including many particles, and by imposing membrane physics on the drop interface. Currently, we have certain of these developments in hand. However, all extensions increase the computational demand of the model. We observe, also, a clear need to formulate a theory, based on supporting experiments, to shed light on the relationship between the way in which the microscopic glycocalyx's constituent complex protein chains are compacted and their subsequent effect on the effective porous viscosity and, hence, on flow.

Acknowledgements

The authors thank Sauro Succi and Andrea Di Mascio for valuable discussions. The technical support from David Rossi is greatly acknowledged. The study was partially supported by the Italian project Interomics.

Notes

1. Email: i.halliday@shu.ac.uk
2. Email: t.j.spencer@shu.ac.uk
3. Email: carola.koenig@brunel.ac.uk
4. Email: collinmw@hotmail.com

References

Arslan N. 2007. Mathematical solution of the flow field over glycocalyx inside vascular system. Math Comput Appl. 12(3):173–179.

Bernaschi M, Melchionna S, Succi S, Fyta M, Kaxiras E, Sircar JK. 2009. MUPHY: a parallel MUlti PHYsics/scale code for high performance bio-fluidic simulations. Comput Phys Commun. 180:1495–1502.

Bouzidi M, Firdaouss M, Lallemand P. 2001. Momentum transfer of a Boltzmann-lattice fluid with boundaries. Phys Fluids. 13(11):3452–3459.

Farhat H, Lee JS, Lee JS. 2011. A multi-component lattice Boltzmann model with non-uniform interfacial tension module for the study of blood flow in the microvasculature. Int J Numer Methods Fluids. 67:93–108.

Guo Z, Zhao TS. 2002. Lattice Boltzmann model for incompressible flows through porous media. Phys Rev E. 66:036304.

Guo Z, Zheng C, Shi B. 2002. Discrete lattice effects on the forcing term in the lattice Boltzmann method. Phys Rev E. 65:046308.

Halliday I, Hollis AP, Care CM. 2007. Lattice Boltzmann algorithm for continuum multicomponent flow. Phys Rev E. 76:026708.

Janoschek F, Toschi F, Harting JDR. 2010. Simplified particulate model for coarse-grained hemodynamics simulations. Phys Rev E. 82(5):056710-1/11.

Kim SH, Pitsch H. 2007. A generalized periodic boundary condition for lattice Boltzmann method simulation of a pressure driven flow in a periodic geometry. Phys Fluids. 19:108101.

Krüger T, Varnik F, Raabe D. 2011. Efficient and accurate simulations of deformable particles immersed in a fluid using a combined immersed boundary lattice Boltzmann finite element method. Comput Math Appl. 61:3485–3505.

Melchionna S. 2011. A model for red blood cells in simulations of large-scale blood flows. Macromol Theory Simul. 20:548–561.

Pahakis MY, Kosky JR, Dull RO, Tarbell JM. 2007. The role of endothelial glycocalyx components in mechanotransduction of fluid shear stress. Biochem Biophys Res Commun. 355(1):228–233.

Pontrelli G, Halliday I, Spencer TJ, Care CM, König CS, Collins MW. 2011. Near wall hemodynamics: modeling the glycocalyx and the endothelial surface. Proceedings of Micro and Nano Flow, MNF2011; 22–24 August 2011; Thessaloniki.

Pontrelli G, König CS, Halliday I, Spencer TJ, Collins MW, Long Q, Succi S. 2011. Modelling wall shear stress in small arteries using the Lattice Boltzmann method: influence of the endothelial wall profile. Med Eng Phys. 33(7):832–839.

Pries AR, Secomb TW. 2008. Blood flow in microvascular networks. In: Handbook of physiology, the cardiovascular system, microcirculation. Bethesda (USA): Am. Phys. Soc.

Reichlin T, Wild A, Dürrenberger M, Daniels AU, Aebi U, Hunziker PR, Stolz M. 2005. Investigating native coronary artery endothelium *in situ* and in cell culture by scanning force microscopy. J Struct Biol. 152:52–63.

Secomb TW, Hsu R, Pries AR. 2002. Blood flow and red blood cell deformation in nonuniform capillaries: effects of the endothelial surface layer. Microcirculation. 9:189–196.

Succi S. 2001. Lattice Boltzmann equation for fluid dynamics and beyond. Oxford, UK: Oxford University Press.

Van Doormal MA, Zhang J, Wada S, Shaw JE, Won D, Cybulsky MI, Yip CM, Ethier CR. 2009. Variations in mass transfer to single endothelial cells. Biomech Model Mechanobiol. 8(3):183–193.

Vincent PE, Sherwin SJ, Weinberg PD. 2008. Viscous flow over outflow slits covered by an anisotropic Brinkman medium: a model of flow above interendothelial cell cleft. Phys Fluids. 20(6):063106.

Wada S, Karino T. 2002. Prediction of LDL concentration at the luminal surface of a vascular endothelium. Biorheology. 39:331–336.

Waters, SL, Alastruey, J, Beard, DA, Bovendeerd, PHM, Davies PF, Jayaraman, G, Jensen, OE, Lee, J, Parker, KH, Popel, AS, Secomb, TW, Siebes, M, Sherwin, SJ, Shipley, RJ, Smith, NP, van de Vosse, FN. 2011. Theoretical models for coronary vascular biomechanics: progress & challenges. Prog Biophys Mol Biol. 104:49–76.

Weinbaum S, Tarbell JM, Damiano ER. 2007. The structure and the function of the endothelial glycocalyx layer. Annu Rev Biomed Eng. 9:121–167.

Yao Y, Rabodzey A, Forbes Dewey C, Jr. 2007. Glycocalyx modulates the motility and proliferative response of vascular endothelium to fluid shear stress. Am J Physiol Heart Circ Physiol. 293:H1023–H1030.

Zhang J, Johnson PC, Popel AS. 2008. Red blood cell aggregation and dissociation in shear flows simulated by lattice Boltzmann method. J Biomech. 41:47–55.